I&EC research
Industrial & Engineering Chemistry Research

Article

pubs.acs.org/IECR

Numerical Investigation on the Effect of Pressure on Fluidization in a 3D Fluidized Bed

Vikrant Verma, Johan T. Padding,* Niels G. Deen, and J. A. M. (Hans) Kuipers

Multiphase Reactors Group, Department of Chemical Engineering and Chemistry, Eindhoven University of Technology, P.O. Box 513, 5600 MB Eindhoven, The Netherlands

ABSTRACT: We apply a two-fluid model to investigate hydrodynamic differences in a three-dimensional fluidized bed operating at pressures of 1, 2, 4, 8, 16, 20, and 32 bar. The simulation results are compared with experimental results from the literature and show very good agreement. A detailed investigation is carried out on pressure fluctuations, porosity distribution, and bubble and solids flow characteristics. At high pressure, the porosity distribution is homogeneous and fluidization is smooth. The bubble size depends upon the location in the 3D bed, showing different trends at different pressures. The average bubble size is reduced with an increase in pressure, caused by a difference in coalescence and splitting of bubbles. An initial increase in pressure from 1 to 2 bar shows an increase in bubble rise velocity, but a further increase in pressure causes bubbles to rise more slowly. High up-flow of solids is observed in the center at high pressures, with pronounced differences in solids circulation vortices.

INTRODUCTION

Gas−solids fluidized beds (FBs) are extensively used in the process industries because of their distinct capabilities as a reactor and mixer and the possibility of continuous operation. A lack of understanding of the fundamentals of dense gas−solids flows in general has led to several difficulties in the design and scale-up of these reactors.[1] Difficulties can be associated with operating conditions and/or reactor dimensions. For example, industrial fluidized beds for the production of polymers are operated at pressures of about 20 bar, while research on fluidized beds is generally performed at atmospheric conditions. Understanding of the hydrodynamics for pressurized FB systems is lacking and deserves more detailed investigation. The performance of a fluidized bed is strongly governed by the formation of gas bubbles and their distribution, facilitating rapid solids mixing and high heat transfer rates to immersed surfaces. The initial formation and propagation of gas bubbles in fluidized beds not only depend upon the properties of the solid material and inlet gas velocity but also on bed operating conditions, such as pressure and temperature.

The properties of a fluidized bed can be tuned to achieve optimal contact between the phases, by regulating the bubble size and hence the bubble-to-emulsion mass transfer rates. Yet controlling the bubble size is not an easy process, because it depends highly upon the operating conditions of the bed.[2] A reduction in bubble size at high pressure is well-known in the literature.[3−6] However, the hydrodynamics of pressurized systems is not fully understood. Fluidization at elevated pressures requires a detailed understanding and hence remains an active area of research. In general, the effect of pressure on minimum fluidization velocity, bed voidage, and bed expansion have been reported extensively in the literature.[7,8] The minimum fluidization velocity decreases with an increase in pressure. Primarily, this is caused by the increase in gas density with an increase in pressure at constant temperature, according to the ideal gas law. The effect of gas pressure on gas phase viscosity is very weak and is usually ignored.[9] However, in fluidized beds, the influence of pressure cannot be explained in terms of gas phase density only, as solids of different types behave differently under similar operating condition. For Geldart A particles, pressure does not have any significant effect on minimum fluidization velocity.[3,10] However, for coarse particles (Geldart B/D), the minimum fluidization velocity decreases with an increase in pressure, whereas the dense phase voidage remains unaffected.

Industrial fluidized beds are mostly operated at a superficial gas velocity well above the minimum fluidization velocity.[11] Therefore, these parameters are of less importance on an industrial scale. In such reactors, the motions of the bubble and solids are key factors to determine reactor performance. In previous studies, information obtained from pressure fluctuations has been used to determine flow regimes at elevated operating pressure, because direct visual access is difficult.[4] Olowson and Almstedt[8,12,13] have extensively studied characteristics of bubbles at elevated pressures. They reported[12] that an increase in pressure may cause either an increase or a decrease in bubble size, depending upon the location in the bed and the pressure level. Similar observations have been reported by other researchers for various solids materials. However, these complex structures of bubbles and solids motion at elevated pressures are not properly understood. A major factor is that flow visualization and measurements at elevated pressure are noticeably difficult to perform. Nevertheless, researchers[6,14,15] have applied advanced tomographic techniques to capture the bubble dynamics at high pressure. Godlieb et al.[14] studied a 0.30 m diameter fluidized bed using electrical capacitance tomography (ECT) at operating pressures ranging from 1 to 20 bar. They observed similar changes in bubble activity with an

Received: June 19, 2014
Revised: September 29, 2014
Accepted: October 8, 2014
Published: October 8, 2014

increase in pressure. By constructing a probability density function of the porosity, they were able to show that the bed attains a state of homogeneous flow of gas and solids at very high pressure. They also observed a significant increase in porosity at the center of the bed with an increase in pressure. However, a detailed understanding of bubble and solids motion is still lacking in their work, due to the poor resolution of the ECT measurements. Brouwer et al.[15] applied a fast X-ray tomography technique to study bubble dynamics in a 0.25 m diameter column at operating pressures ranging from 1 to 5 bar. They observed a continuous reduction in bubble size with an increase in pressure within this range. They tried to fit the detected spherical equivalent bubble diameter with the correlation developed by Darton et al.[16] using the catchment area A_0 as a fitting parameter in the correlation.

So far, bubble characteristics at high pressure are known to a certain extent. However, to our knowledge, no information on solids circulation is available in the literature for pressurized fluidized beds. Furthermore, almost all studies available in the literature on the effect of pressure on fluidization are concerned with pressure fluctuations from experimental measurements. No numerical study has been performed to predict the flow dynamics at elevated pressures in a bench-scale fully three-dimensional fluidized bed. Note that the work of Godlieb[28] is concerned with a very small pseudo-2D fluidized bed 2.5 cm in diameter, possibly due to the high computational costs. Fortunately, with increasing computational power, it has become possible to use numerical simulations to predict the flow dynamics at elevated pressure in 3D FBs.

In this work, we use a two-fluid model (TFM), based on the kinetic theory of granular flow, to investigate the effect of operating pressure on bubble and solids flow characteristics. Operating pressures of 1, 2, 4, 8, 16, 20, and 32 bar are studied with particles of Geldart B classification, having a diameter of 1.1 mm and a density of 800 kg/m^3, in a 0.30 m diameter column. Because for Geldart B particles the minimum fluidization velocity decreases with increasing pressure, a comparison is made at a constant excess gas velocity equal to the minimum fluidization velocity at 1 bar.

This paper is organized as follows. First, a short description of the TFM is given, focusing on the main governing equations. Then, the results are presented, including details of the simulation settings, validation, and a discussion of the results. We finish with our conclusions.

TWO-FLUID MODEL

The two-fluid continuum model describes both the gas phase and the solids phase as fully interpenetrating continua using a generalized form of the Navier–Stokes equations.[17,18] To account for particle–particle interactions, the kinetic theory of granular flow[19,20] (KTGF) is used. In this work, the standard TFM equations were used to describe the continuum modeling approach for the gas and solids phases. The conservative equations for the KTGF model are based on the work of Nieuwland,[20] as referenced by Verma et al.[21] Further details of the two-fluid model used in this work, and the approach to efficient numerical solution in cylindrical coordinates, have been reported extensively by Verma et al.,[21] who have also have presented a thorough validation of our TFM by comparing the bubble characteristics in a 0.10 m diameter bed for different granular materials and comparing those characteristics with experimental X-ray tomography results.[22]

PARAMETER SETTINGS

In this work, the choice of bed material and operating conditions corresponds to those of the experimental study by Godlieb et al.[14] They performed experiments at elevated pressure of 1, 2, 4, 8, 16, and 20 bar using electrical capacitance tomography on a bed of diameter 0.30 m, with linear low-density polyethylene (LLDPE) particles as fluidization material. They compared different operating pressures using a constant excess gas velocity, as well as 3 times the minimum fluidization velocity. In our work, we will specifically compare fluidization at different pressures using a constant excess gas velocity, to preserve similar flow conditions. Additionally, we will also investigate the fluidization behavior at a very high operating pressure of 32 bar. The drag force model and frictional stress model used in this work are from Van der Hoef et al.[23] and Srivastav and Sundaresan,[24] respectively. The values of density, diameter, and coefficient of restitution for LLDPE particles are set to 800 kg/m^3, 1.1 mm, and 0.69, respectively. The fluidized bed dimensions, with details of the computational grid size, are presented in Table 1. The above-mentioned particle properties and the bed dimension as given in Table 1 are kept the same for all operating pressures. The parameters that vary with pressure, i.e., minimum fluidization velocity and inlet gas velocity, are given in Table 2. We performed simulations for a total time of 10.0 s. Time-averaging was performed by ignoring the initial first second to avoid inclusion of start-up effects.

Table 1. Bed and Grid Size Specification

bed diameter	0.30 m
overall height of the domain	1.20 m
initial particle bed height	0.60 m
number of grids in the r-direction	30
number of grids in the θ-direction	24
number of grids in the z-direction	240

Table 2. Mimimum Fluidization Velocity (U_{mf}) and Gas Velocity ($U_{mf} + U_{mf,1bar}$) at Different Pressures

pressure (bar)	U_{mf} (m/s)	$U_{mf} + U_{mf,1bar}$ (m/s)
1	0.30	0.59
2	0.25	0.54
8	0.15	0.45
16	0.11	0.41
20	0.10	0.40
32	0.097	0.397

RESULTS AND DISCUSSION

Pressure Fluctuations. Analysis of pressure fluctuations in fluidized beds is common in past studies of fluidized bed hydrodynamics.[25−27] Because optical accessibility of pressurized systems is difficult, information on pressure fluctuations is often used to derive the bubble and solids motion. Due to the lower pressure inside bubbles and their continuous passage through the bed, the pressure drop measured over the full bed height is continually fluctuating.[28,29] The strength of these fluctuations depends upon the activity of bubbles in the bed and phenomena such as coalescence and splitting of bubbles.[6] Goldschmidt[29] reported that a strong intensity in pressure drop fluctuations indicates more vigorous bubbling of the fluidized bed. Different fluidization regimes are identified with a change

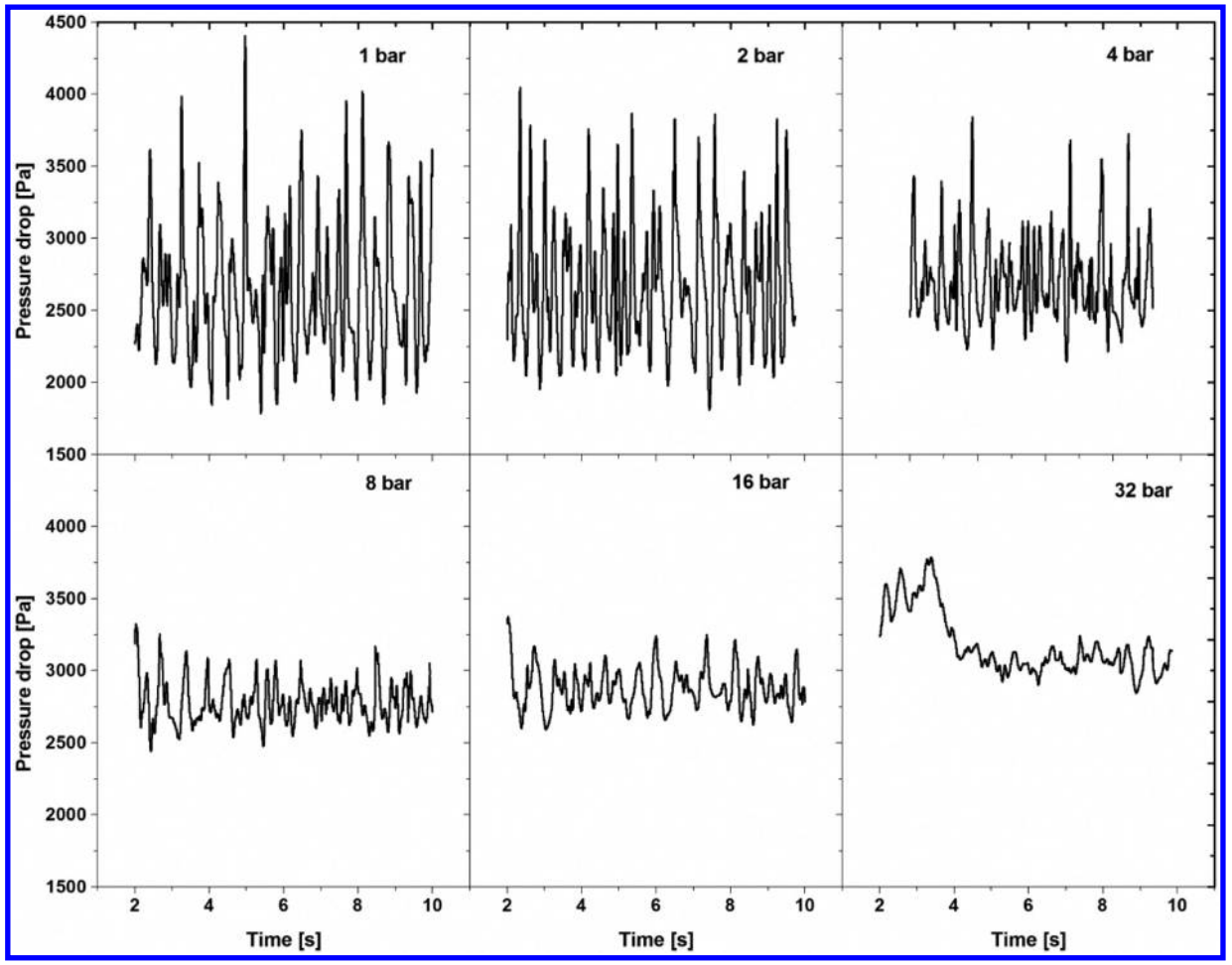

Figure 1. Pressure drop fluctuations over the bed with time for different operating pressures.

in characteristics of the pressure fluctuations (Cai et al.[30]). Figure 1 shows the pressure drop (across the whole bed) fluctuations, averaged over the cross-section of a fluidized bed at different operating pressures. The pressure fluctuation intensity is strong at an operating pressure of 1 bar, and the intensity decreases as pressure is increased. The intensity of pressure fluctuations at a pressure of 32 bar is very weak. This indicates that at high pressure the fluidization is smooth and bubbles cannot be distinguished from the emulsion phase. A similar analysis on the basics of pressure fluctuations at different operating pressures was made by Orta et al.[6] We will return with details on the actual bubble behavior in later sections.

By applying a fast Fourier transformation (FFT) to the time series of pressure fluctuations shown in Figure 1, the pressure fluctuation power spectrum can be obtained, as shown in Figure 2. The power spectra show a decreasing trend with an increase in pressure, in agreement with our previous observation that pressure fluctuations decrease with increasing pressure, indicating different bubbling behavior in the fluidized bed at different operating pressures. Multiple peaks are seen in the spectra. These peaks are commonly encountered in bubbling fluidized beds, as explained by Brown and Brue,[25] and Orta et al.[6] Figure 2 shows that the dominant frequency of pressure fluctuations lies between 0 and 1 Hz. This observation is consistent with experimental results reported in the literature.[6]

General Bubble Characteristics. Figure 3 shows instantaneous snapshots of porosities for a vertical plane cutting through the center of the 3D bed for different operating

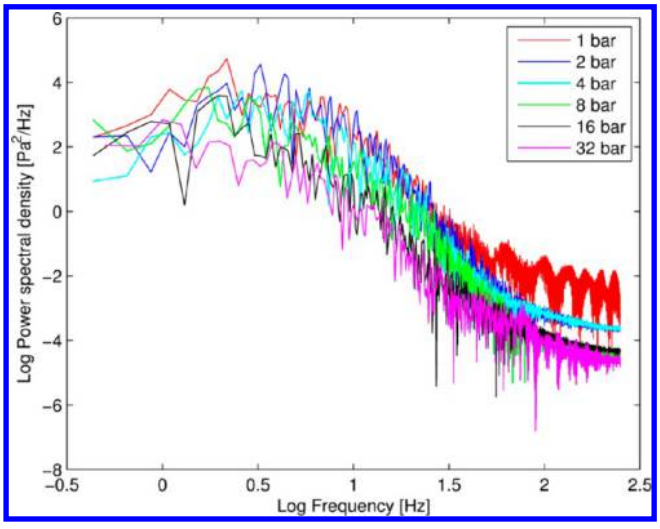

Figure 2. Power spectral density of the pressure drop fluctuation for different operating pressures.

pressures. This figure clearly shows that the hydrodynamics is changing with a change in operating pressure. Bubbles are easy to distinguish from the emulsion phase at lower pressures. However, at high operating pressures the bubbles are of very random shape and lose their identity. At lower pressures, mostly the bubbles are initiated near the wall and move toward the center of the bed. A notable difference is seen at high

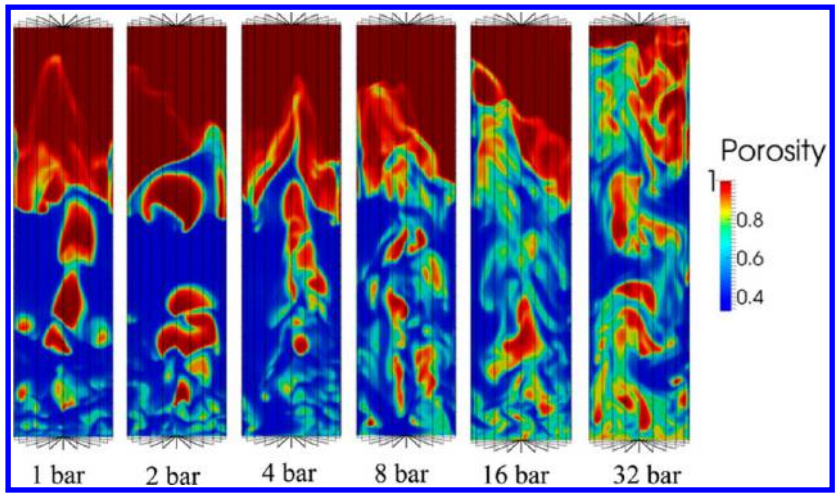

Figure 3. Instantaneous snapshots of porosity plots in the vertical plane that lies in the middle of the 3D bed.

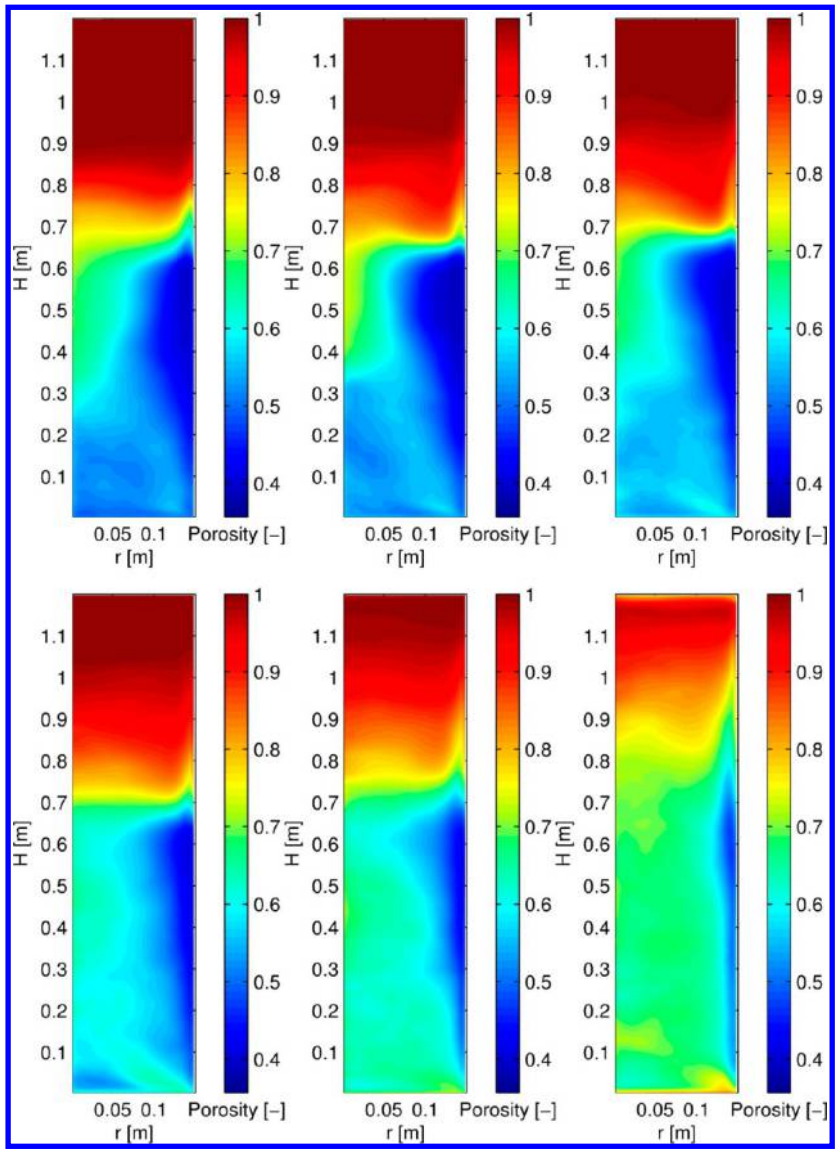

Figure 4. Azimuthally and time-averaged porosity contours at different operating pressures (top, left to right, 1, 2, and 4 bar; bottom, left to right, 8, 16, and 32 bar).

pressures, where the bubble flow and distribution is uniform throughout the cross section of the bed. Fluidization at high pressure is smooth, and bubbles are difficult to distinguish from the emulsion phase.

dx.doi.org/10.1021/ie502474k | *Ind. Eng. Chem. Res.* 2014, 53, 17487−17498

Porosity Distribution. Figure 4 shows the azimuthally and time-averaged porosity plots. At the lower operating pressures of 1, 2, and 4 bar, only small differences in porosity are seen, mainly in the center. An abrupt change in porosity distribution is seen when the pressure is increased from 4 to 8 bar. The central region of the bed is almost homogeneous at 8 bar, with thick solids shear zones near the side walls. At 16 bar, the layer of solids near the side walls is diminished and the porosity is homogeneous throughout the bed. This shows that the activity of bubbles in the center is increased as pressure is increased, predominantly in the bottom section of the bed. With an increase in pressure the effect on the porosity distribution starts to grow from the center. The porosity is uniformly distributed at a pressure of 32 bar. Parts a and b of Figure 5 compare the average porosity for different operating pressures at a fixed height from the bottom. Figure 5a shows a relatively small difference in porosity at 1, 2, and 4 bar and a sudden change occurring when the pressure is further increased to 8, 16, and 32 bar. In Figure 5b, the porosity in the central region (r = 0 to 5 cm) is higher for an operating pressure of 1 bar than at 2 and 4 bar. This is because at this height bubbles reach the center of the bed. Note that the porosity profile is almost flat and uniform throughout the cross-section at the pressure of 32 bar. This again shows that fluidization is uniform at the highest pressure.

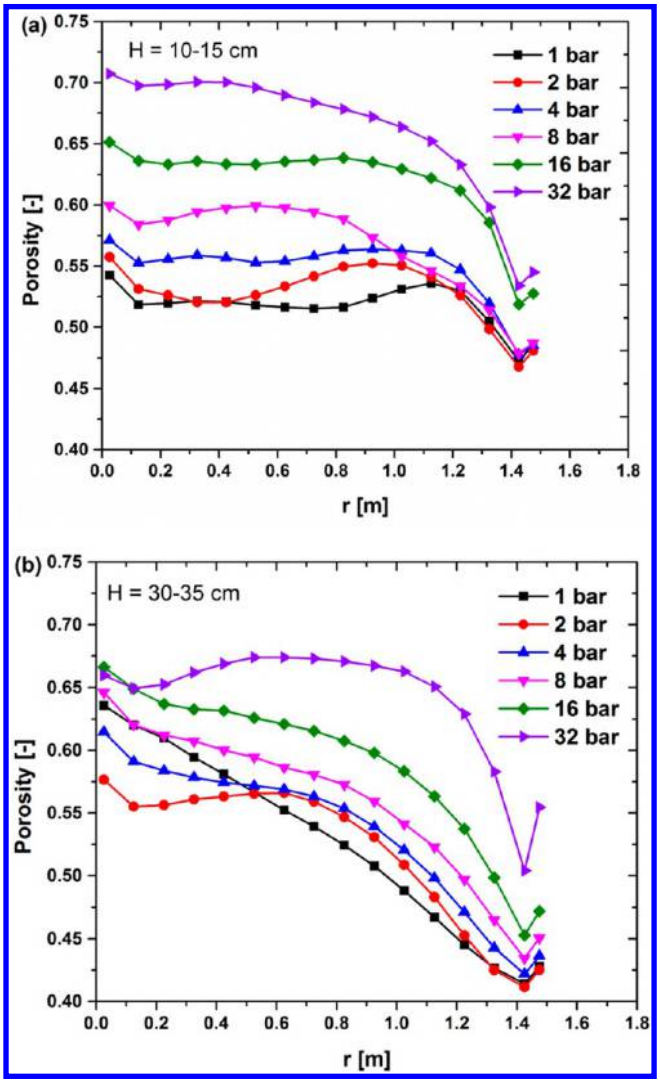

Figure 5. Azimuthally and time-averaged porosity as a function of radial position, compared for different operating pressures at heights between (a) 0.1 and 0.15 m and (b) 0.3 and 0.35 m, from the bottom.

The probability density function (PFD) of porosity quantifies the relative occurrence of porosities in the emulsion phase and the bubble phase. To obtain the PDF a small porosity bin size of 0.01 was used, and the variable cell size in the computational cylindrical domain is properly taken into account. Figure 6a–c shows the PDF at different axial positions, comparing different operating pressures. These figures show a decrease in dense phase and an increase in emulsion and bubble phase as the pressure is increased. The smallness of the dense phase peak at an operating pressure of 32 bar indicates that the porosities are uniformly distributed. These results on porosity distribution are consistent with the experimental work of Godlieb et al.[14] A distinct behavior is seen in the PDF plot when the pressure is increased from 1 to 2 bar, with a higher dense/emulsion phase peak at 2 bar (Figure 6b,c). This rise in dense phase peak from 1 to 2 bar is also observed in the experimental results of Godlieb et al.[14] We will quantify the behavior in this pressure range in a later section on bubble characteristics.

Sharp bubble peaks do not occur in the PDFs, particularly at lower heights. This is due to the fact that bubbles are small at the bottom and that these bubbles are surrounded by emulsion and/or dense phase. In 3D, the frequency of occurrence of a dense/emulsion phase is higher than for a bubble phase. This is also clear from the porosity contours in Figure 3, which show a high solids shear zone in the bottom of the bed at low operating pressures. Godlieb et al.[14] reported that the missing of a bubble peak could be due to the low resolution of the ECT technique. However, our simulations show the same porosity distribution in the bubble zone, revealing that this is a true property of a 3D fluidized bed and not a limitation of ECT. In another study, Godlieb et al.[31] performed DPM simulations at high pressure for a 2D fluidized bed, where a bubble peak was clearly visible in the porosity PDF. We now attribute this to the fact that the bubbles are surrounded by a less dense/emulsion phase because of the missing third dimension.

In parts a and b of Figure 7 the porosity PDF is shown at different heights for operating pressures of 1 and 20 bar, respectively. At 1 bar we observe that with an increase in height from the bottom, the emulsion phase is getting denser. This is caused by continuous gas extraction by the bubble from the emulsion phase as they grow in size due to coalescence. A similar trend is observed at 20 bar, with the difference that the curves are shifted to higher porosity values. At the lowest plane just above the bottom inlet domain, at 20 bar the porosity distribution is broad with the maximum peak shifted to 0.7. This shows that neither a distinct emulsion phase nor a distinct bubble phase is observed at this height. All these prediction from our simulations are consistent with the experimental results of Godlieb et al.[14]

According to the two-phase theory originally proposed by Toomey and Johnstone,[32] an excess of gas is responsible for the formation of bubbles. This implies that at different operating pressures a constant bubble hold-up would be predicted, with the assumption that bubble coalescence and breakup do not depend upon operating pressure. However, we observe that at constant excess gas velocity the bubble hold-up is increasing with an increase in operating pressure. This shows that a change in bubble properties is occurring at high operating

dx.doi.org/10.1021/ie502474k | Ind. Eng. Chem. Res. 2014, 53, 17487–17498

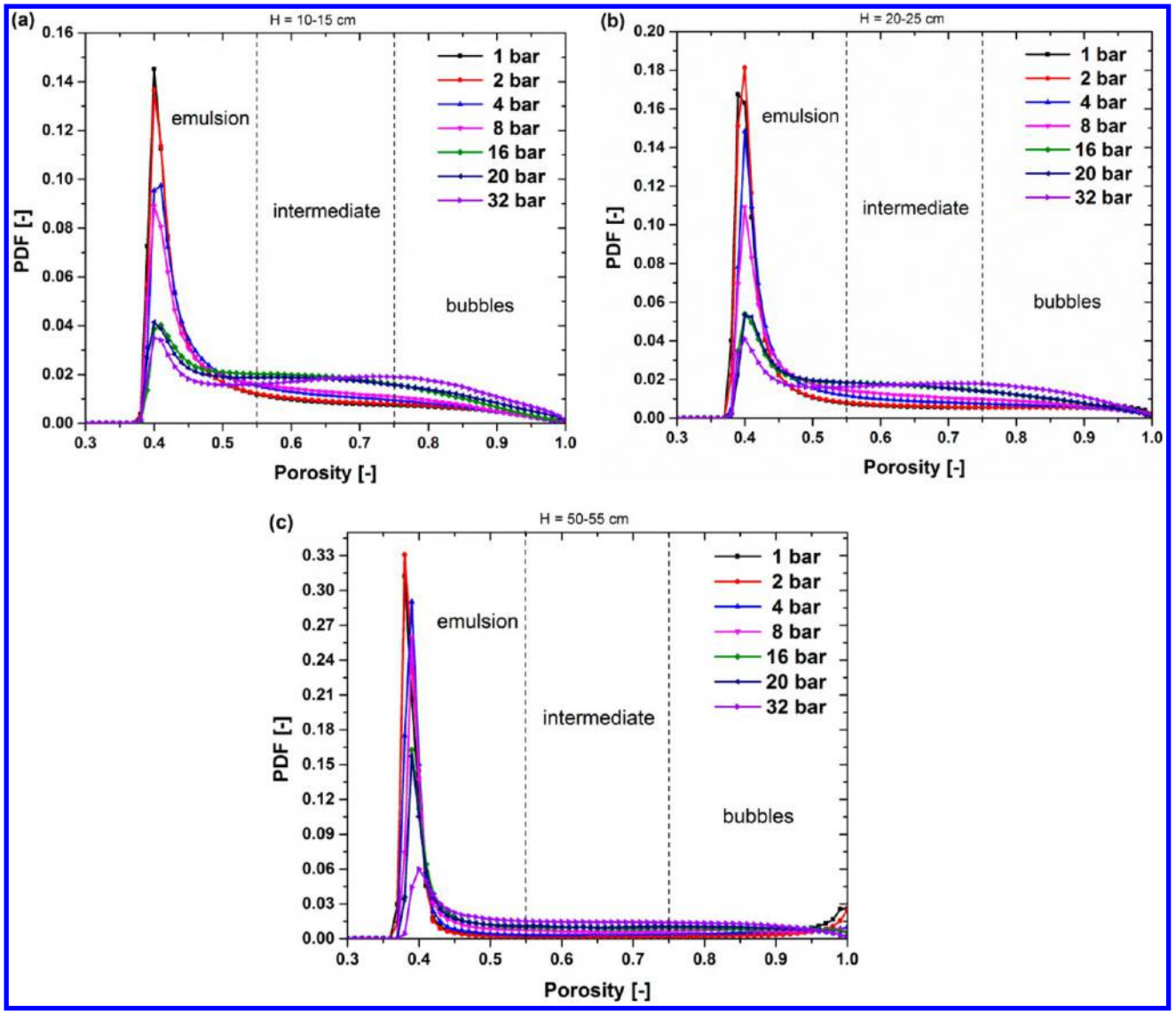

Figure 6. PDF of time-averaged porosity compared for different operating pressures between the heights of (a) 0.10 and 0.15 m, (b) 0.20 and 0.25 m, and (c) 0.5 and 0.55 m, from the bottom.

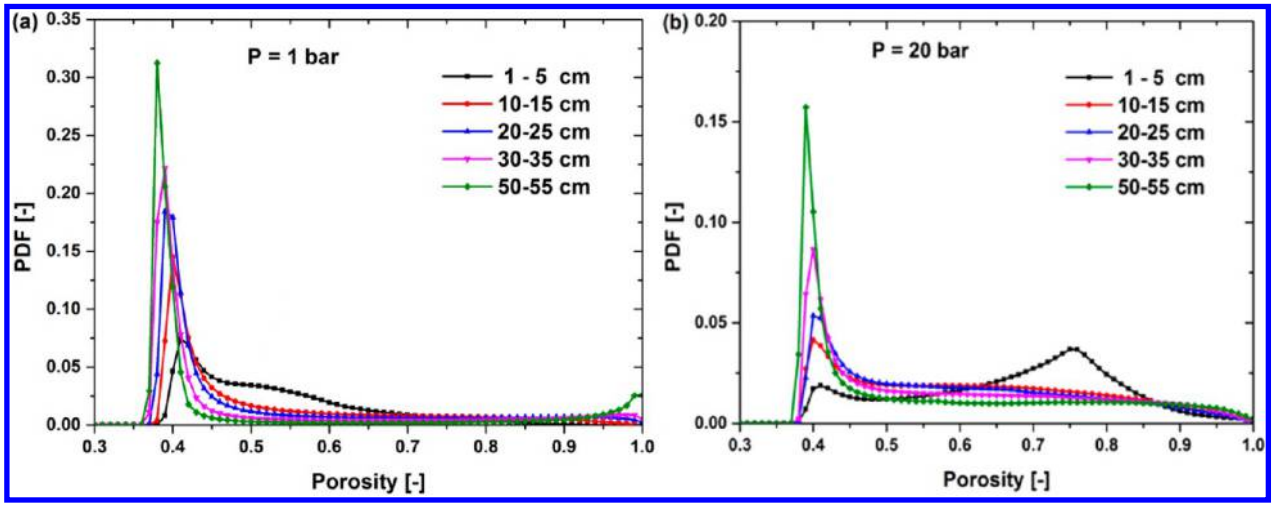

Figure 7. PDF of time-averaged porosity at several heights from the bottom for operating pressures of (a) 1 bar and (b) 20 bar.

pressure. Details on the bubble characteristics are discussed in the next section.

Bubble Size. To calculate the bubble characteristics, we use information on the gas volume fraction (porosity), available for

dx.doi.org/10.1021/ie502474k | Ind. Eng. Chem. Res. 2014, 53, 17487−17498

each computational cell in the domain of interest. A porosity value larger than 0.75 is designated as a bubble cell. A sophisticated technique is used to identify the cells belonging to an individual bubble. A linear interpolation of porosities is used to calculate the precise location of the bubble boundary in the sharp gradient between the bubble and emulsion phase. The individual 3D bubble volume (V) is used to calculate the equivalent bubble diameter (D_{e3D}), based on a spherical bubble of equal volume (eq 1). The average bubble diameter is obtained from the total number of predicted bubbles.

$$D_{e3D} = \sqrt[3]{\frac{6V}{\pi}} \quad (1)$$

Figure 8 shows a sharp increase in the equivalent bubble diameter with height for operating pressures of 1, 2, and 4 bar.

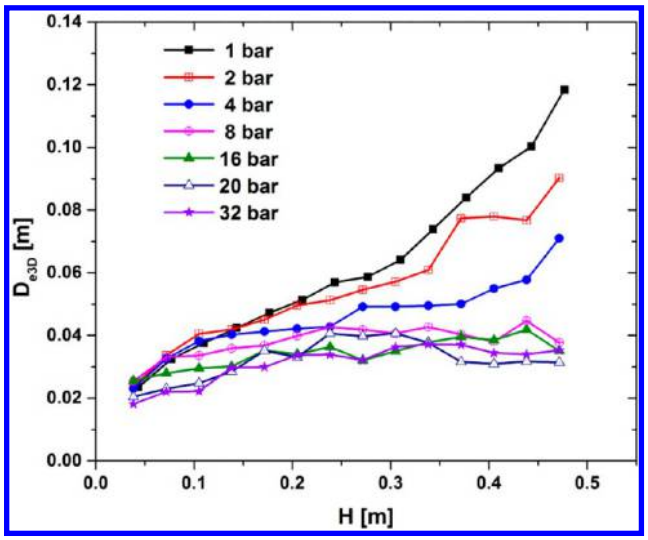

Figure 8. Averaged equivalent bubble diameter as a function of height from the bottom, compared for different operating pressures.

However, for operating pressures of 8, 16, 20, and 32 bar a relatively small increase in the bubble diameter is predicted with an increase in height from the bottom. Comparing bubble sizes for different operating pressures, the average bubble size decreases with an increase in pressure, where significant differences are observed in the top section of the bed. A substantial decrease in bubble size is seen when the pressure is increased from 1 to 2 bar. Comparing results from 2 to 4 bar and from 4 to 8 bar, a further increase in pressure leads to almost the same bubble size. A decrease in bubble diameter at all axial positions with increase in pressure from 1 to 5 bar is also reported by Brouwer et al.[15]

Coalescence and breakup of bubbles are well-known phenomena in FBs. These phenomena are complex to understand and depend upon many factors, such as solids material, fluidizing gas velocity, and operating conditions. The PDF plots in Figure 6 show an increasing gas hold-up with an increase in pressure. This confirms that the decrease in average bubble size at high pressure is due to the dominance of the bubble breakup phenomena. Figure 9 shows a series of snapshots at an operating pressure of 16 bar, revealing splitting (marked circles/ellipses) and coalescence (marked squares) phenomena. Splitting of bubbles due to an instability of bubbles at high operating pressure is also reported in the literature.[5,32] Wiman and Almstedt[5] explained that the increase in gas−particle interaction and turbulent fluctuation in the gas phase at high pressure can cause bubble splitting and dense phase expansion. They also observed that the through-flow velocity of gas through bubbles decreases with increasing pressure, probably due to the decrease in minimum fluidization velocity, limiting the growth in size of the bubbles. This is consistent with our simulation predictions. The small bubbles are also consistent with the pressure fluctuation analysis performed previously in this paper (Figure 1).

Figure 10 shows the azimuthally averaged bubble size as a function of radial position. The bubble size is approximately the same near the wall region and decreases with an increase in pressure in the annulus region. However, in the central region of the bed, the bubble size increases with increasing operating pressure. This is due to an increase in activity of bubbles in the center at high pressure. Olowson and Almstedt[12] reported that an increase in pressure may cause either an increase or a decrease in bubble size, depending upon the location in the bed and the pressure level. It is also clear from our simulations that bubbles can behave differently at different operating pressures, depending upon their location in the 3D bed. Olsson et al.[4] studied bubble properties for a pressure range of 1−16 bar. They observed that the bubble pierced length initially increases to a maximum value and then decreases with increasing pressure. Similar observations are reported by Olowson and Almstedt,[12] and Hoffmann and Yates.[33] From our simulation results, this behavior is predicted mainly in the bottom section (below 0.10 m) and annulus region (between r = 0 to 0.06 m) of the bed, as seen from Figures 8 and 10, respectively. The bubble size increases as the pressure is increased from 1 to 2 bar, yet further increase in pressure causes a slight reduction in bubble size. One could argue that this narrow difference is within the standard error of the simulation results. However, we also observed a clear distinction in the bubble rise velocity at these pressures, which we will discuss later. Olsson et al.[4] concluded that this nonmonotonous behavior is caused by a combined effect of pressure and fluidization velocity on the bubble size. When inertial forces dominate over the viscous forces, bubbles become unstable, resulting in splitting. Cai et al.[30] also concluded that at low gas velocity there is a dual effect of pressure on bubble size; i.e., initially the bubble size increases with an increase in pressure up to 10 bar and the bubble size decreases upon further increase in pressure. In our simulation for a constant excess gas velocity of 0.30 m/s, this state occurs at a pressure less than 4 bar, mainly in the bottom section and in the center of the bed.

Bubble Aspect Ratio. The shape of the bubbles can be estimated from the bubble aspect ratio, defined as the ratio of the vertical length of the bubble to its horizontal length. Figure 11a shows the change in the bubble aspect ratio with height from the bottom, revealing that with increasing height from the bottom the bubble the aspect ratio increases for all operating pressures. Flat bubbles are predicted in the bottom section of the bed. At a fixed height, the bubble aspect ratio increases with increasing pressure for pressures up to 8 bar and remains almost constant with a further increase in pressure. At pressures above 8 bar, the distinction between bubble and emulsion phase is not clear, which makes it difficult to define the shape of a bubble. This explains the fluctuating trend in bubble aspect ratio observed above an operating pressure of 8 bar.

Figure 11b shows the bubble aspect ratio as a function of bubble diameter, for different operating pressures. A decreasing trend in bubble aspect ratio with increasing bubble diameter is

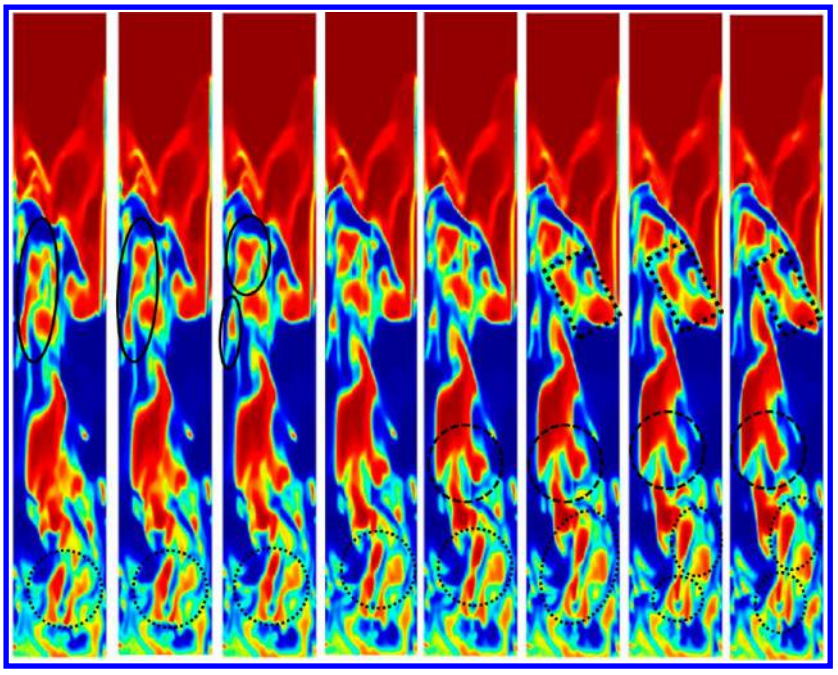

Figure 9. Series of snapshots of porosity plots in the vertical plane that lies in the middle of 3D bed at an operating pressure of 16 bar. Splitting and coalescence of bubbles are highlighted, where circular/elliptical highlighted regions show splitting of bubbles and square boxes show coalescence of bubbles.

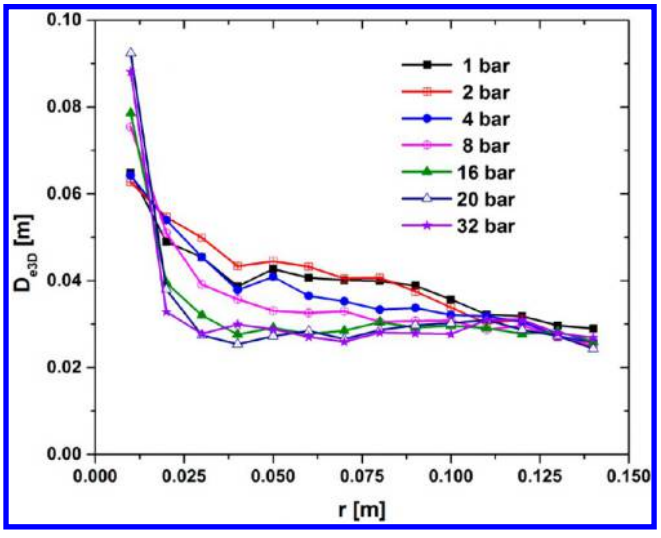

Figure 10. Azimuthally and time-averaged equivalent bubble diameter, averaged over the entire bed at given radial position, compared at different operating pressures.

predicted, irrespective of operating pressure. Only at lower pressures of 1, 2, 4, and 8 bar, a substantial decrease in bubble aspect ratio is seen. For pressures of 16, 20, and 32 bar, the bubbles are elongated and do not attain a spherical shape. Overall this shows that larger bubbles are flat at low pressure and elongated at high pressure.

Figure 11a shows that at operating pressures above 4 bar and above a height of 0.20 m, the bubble aspect ratio is nearly constant, close to a value of 1.5. This value is the result of an average over small and large bubbles, with aspect ratios as projected from Figure 11b. This shows the coexistence of smaller and larger bubbles in the higher section of the bed, caused by splitting of larger bubbles. The same is true for lower pressures of 1, 2, and 4 bar with different values for the bubble aspect ratios.

Bubble Rise Velocity. The bubble rise velocity is calculated by a bubble tracking method, in which the displacement of the centroid of each individual bubble is traced. The net vertical movement of the centroid of a bubble with time provides the bubble rise velocity. The average bubble rise velocity is calculated by averaging over all the tracked bubbles.

First we compare the bubble rise velocity with the experimental measurement of Godlieb et al.[14] Figure 12 shows that our simulation results are in close agreement with their experimental observations. The small differences in simulation predictions and experimental measurements can be attributed to the difference in approach of calculating the bubble rise velocity. In the experiments, the bubble rise velocity is obtained from cross-correlating porosity values between two measurement planes separated by a small vertical distance, whereas in the simulations we apply an individual bubble tracking method to obtain the bubble rise velocity. We also suspect that these deviations might be caused by the neglect of tangential and rotational friction in the KTGF model. Nevertheless, the bubble rise velocities do not show significant differences between simulations and experiments.

Figure 13 shows the average bubble rise velocity as a function of height from the bottom, comparing different operating pressures. The bubble rise velocity increases with increasing height from the bottom. At a fixed height, the bubble rise velocity decreases with increasing pressure, except for a pressure increase from 1 to 2 bar. The decrease in bubble rise velocity at higher pressures is due to the decrease in bubble size. The increase in bubble rise velocity predicted for a pressure increase from 1 to 2 bar was also observed in the experiments by Godlieb et al.[14] For high pressures beyond 8 bar, the rate of increase in bubble rise velocity with height is not very significant. At these pressures, the bubbles rise with almost the same velocity throughout the bed. Similar observations at

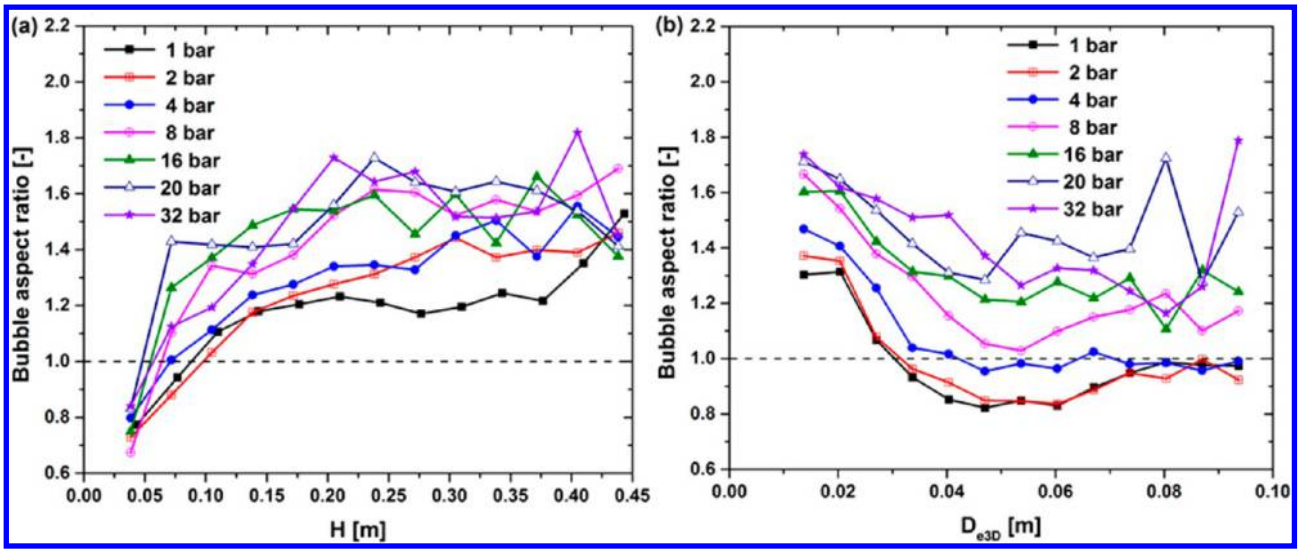

Figure 11. Averaged bubble aspect ratio as a function of (a) height from the bottom and (b) equivalent bubble diameter.

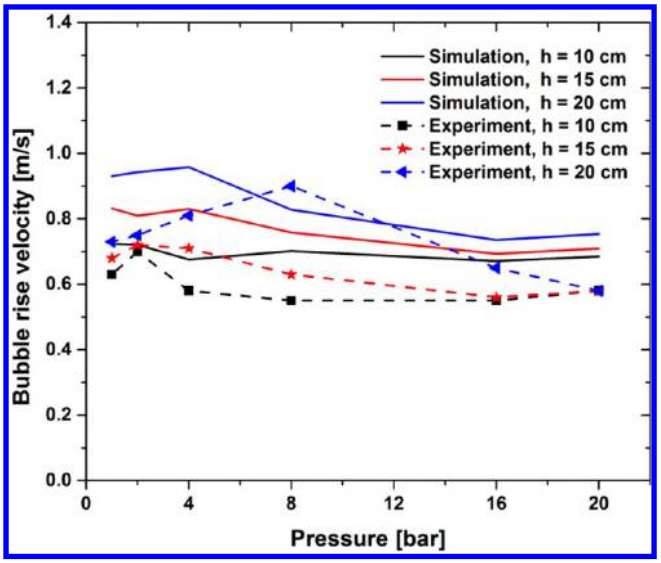

Figure 12. Averaged bubble rise velocity for different operating pressures compared with the experimental results of Godlieb et al.[14]

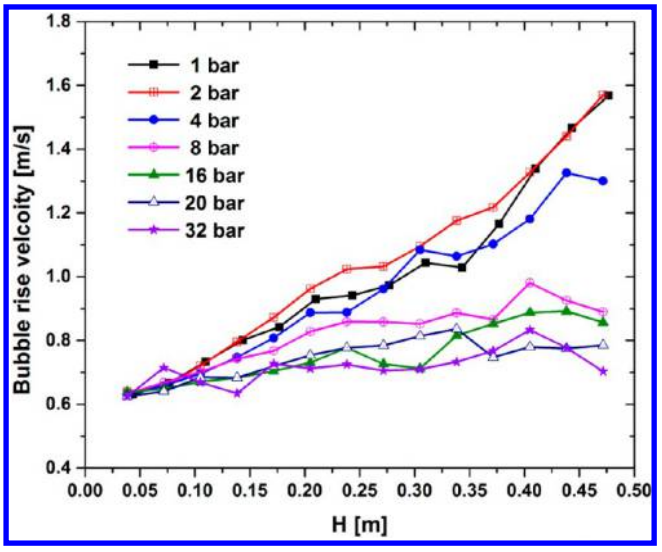

Figure 13. Average bubble rise velocity as a function of height compared for different operating pressures.

20 bar are seen from the experimental measurements of Godlieb et al.[14] (Figure 12), where the bubble rise velocity is nearly the same at three different heights.

Figure 14 shows the bubble rise velocity as a function of radial distance from the central axis, averaged over the entire height of the bed. Again we see a nonmonotonous effect of pressure on the bubble rise velocity. An initial increase in pressure from 1 to 4 bar results in an increase in bubble rise velocity, while a further increase in pressure results in a decrease in bubble rise velocity. Olsson et al.[4] observed an increase in bubble rise velocity in the center of the bed when the pressure is increased. In our simulations this is only true for an increase in pressure from 1 to 4 bar. This might be due to use of a different type of particle at a different operating velocity. Olsson et al. explained that very high pressures caused a central channel motion of bubbles, resulting in high solids circulations and eventually high bubble rise velocities. The central channel of bubbles rising is seen in our simulation animations and also in Figure 3. We will return with details on solids motion in the next section. We do note that at very high pressure, bubbles are not easy to distinguish from the emulsion phase and it becomes difficult to trace individual bubble motion.

Solids Circulation Patterns. Solid particles are dragged up by the bubbles in their wakes, and by continuity, particles will move downward in the regions with no or fewer bubbles. As a consequence, a predominantly downward flow of solids exists in regions of less activity of bubbles, most notably near the side wall. Figure 15 shows the azimuthally and time-averaged solids circulation patterns at different operating pressures. For clarity, not all vectors are shown, but only every alternate vector in the radial direction and axial direction. Also, flashing of particles in the freeboard region is ignored. The simulations predict the appearance of two solids circulation vortices for all operating pressure, with differences in the vortex configurations. The lower solids circulation vortex is nearly the same for operating pressures of 1, 2, and 4 bar, while notable differences at high pressures of 8, 16, and 32 bar are seen. At these high pressures the lower vortex of solids circulation is horizontally elongated. As the pressure is increased, the upper solids circulation vortex

dx.doi.org/10.1021/ie502474k | Ind. Eng. Chem. Res. 2014, 53, 17487−17498

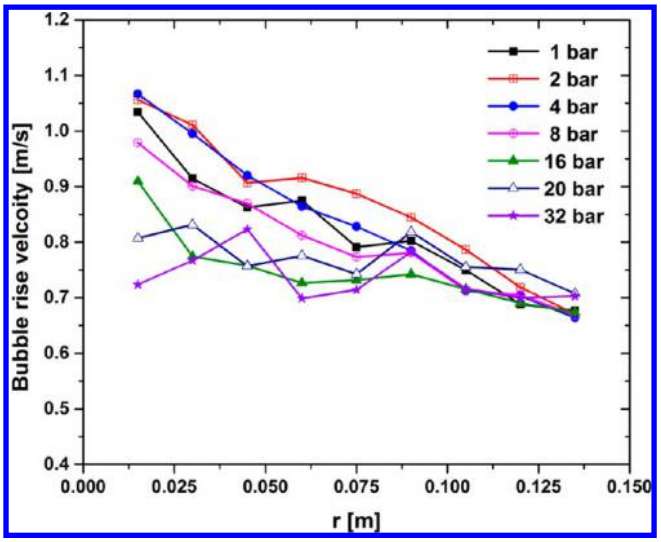

Figure 14. Azimuthally and time-averaged bubble rise velocity, averaged over the entire bed at a given radial position compared for different operating pressures.

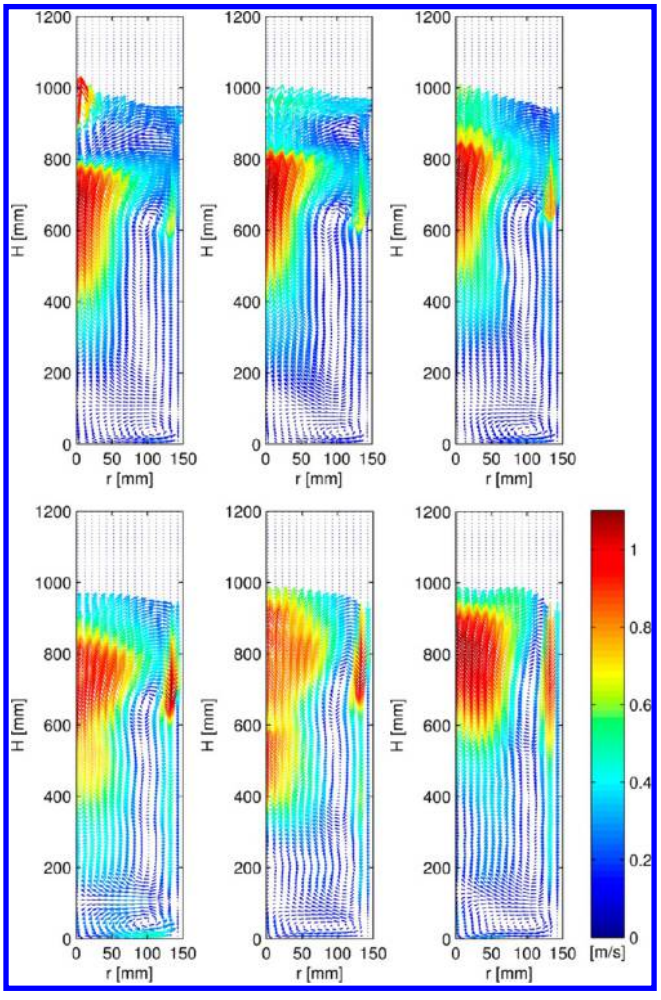

Figure 15. Azimuthally and time-averaged solids circulations at different operating pressures (top, left to right, 1, 2, 4; bottom, left to right, 8, 16, and 32 bar). For clarity, only alternate vectors in radial and axial directions are shown, and splashing of particles in the freeboard region is ignored.

is elongated and the center of this vortex is shifting in height and moving toward the wall. This indicates a high solids circulation at very high operating pressure, where more solids are carried by bubbles in the central region. The rate of down-flowing solids near the wall increases, as seen from the magnitude of the solids velocities in Figure 15. The rise in the center of the upper solids circulation vortices indicates an expansion of the bed at high pressure. Unfortunately, experimental measurements for solids motion at high pressures are not available in the literature. Olowson and Almstedt[12] made an analogy that the increase in bubble rise velocity with increase in pressure is due to a central channel of rising bubbles, causing an increase in solids circulation in the bed. At high pressure, the up-flow of solids through a large cross-sectional area in the center revealed the central channel of rising bubbles.

Parts a–c of Figure 16 show azimuthally and time-averaged solids velocities as a function of radial distance to the central axis at a height of 0.2, 0.4, and 0.6 m, respectively. At a height of 0.2 m from the bottom (Figure 16a), differences in velocity profiles are mainly seen in the center of the bed and near the wall, while no significant difference is seen in the annulus region. At this height, the velocity profile near the wall shows a decreasing trend at the highest pressure of 32 bar. In the center of the bed, the axial solids velocity is increasing as the pressure is increasing from 1 to 2 bar, while a further increase in pressure does not show a clear trend. This might be because the height of 0.2 m lies in between the regions of the lower and upper solids circulation vortices, where the profile is affected by vortex shape. At a height of 0.4 m from the bottom (Figure 16b), the solids velocity shows a clear decreasing trend, both in the center and near the wall, as the pressure is increased. The flatness of the axial velocity profile with an increase in pressure shows that the up-flowing solids in the center are moving with the same axial velocity. At the operating pressure of 32 bar, a uniform profile for upward solids motion is achieved. At a height of 0.6 m from the bottom (Figure 16c), the axial solids velocity increases as the pressure is increased from 1 to 2 bar, while a further increase in pressure results in a decreasing solids velocity in the central region of the bed. This is consistent with our observations of bubble rise velocity. A unique solids velocity profile is predicted for an operating pressure of 32 bar at this height, with a uniform up-flowing solids velocity in the annulus region and a higher magnitude of descending solids velocities near the wall. This is due to a fully homogeneous state, achieved at an operating pressure of 32 bar.

■ CONCLUSIONS

The effect of elevated pressure on pressure fluctuations, porosity distribution, and bubble and solids motion has been investigated in a 3D fluidized bed using a two-fluid model based on KTGF. At high pressures, the porosity distribution is homogeneous and fluidization is smooth. It is observed that with an increase in height from the bottom, the emulsion phase becomes denser at all operating pressures. The location of the peak in the porosity distribution is shifting toward higher porosity with an increase in pressure. At high pressures of 32 bar, the emulsion phase and bubble phase are not easy to distinguish.

A decrease in equivalent bubble diameter is observed with an increase in operating pressure. A substantial decrease is observed for the lower range of pressures, and an almost saturated equivalent bubble diameter is seen at very high operating pressures. The change in bubble diameter with

dx.doi.org/10.1021/ie502474k | Ind. Eng. Chem. Res. 2014, 53, 17487–17498

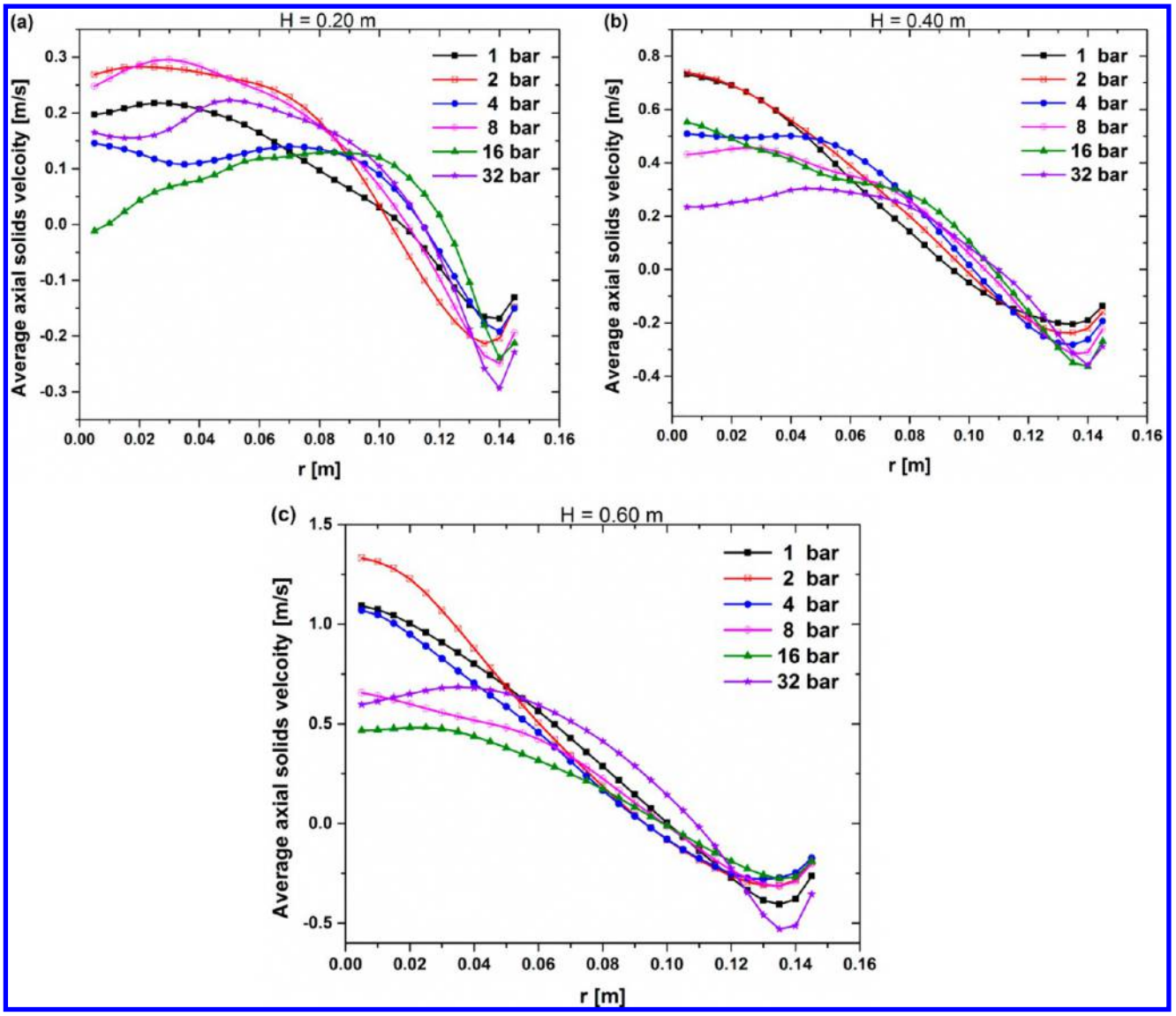

Figure 16. Azimuthally and time-averaged axial solids velocities predicted for different operating pressures and compared at a fixed height of (a) 0.20 m, (b) 0.40 m, and (c) 0.60 m from the bottom.

change in pressure also depends upon the location in the 3D bed. Larger bubbles were predicted at higher pressure in the center of the bed, and conversely, small bubbles were predicted in the annulus region of the bed, with almost the same bubble size near to the wall. This is due to a redistribution of bubbles in the center at high operating pressures. An initial increase in pressure from 1 to 2 bar shows an increase in bubble diameter, while a further increase in pressure results in lowering of the bubble diameter. Similar effects are also seen for the bubble rise velocity, where the bubble rise velocity decreases with an increase in pressure, except when the pressure is increased from 1 to 2 bar. At very high operating pressures, the simulations predict an almost uniform bubble rise velocity throughout the bed. Our results are consistent with results from the literature.

The bubble shape factor at high pressure has been investigated. Our results show that bubbles are vertically elongated as pressure is increased. Bubbles do not attain a spherical shape at operating pressures above 4 bar.

For the first time, the effect of operating pressure on solids circulation has been shown. A uniform up-flow of solids through the center (r = 0−10 cm) has been predicted at very high operating pressure. Also, at high pressure the solids circulation vortex in the bottom of the bed is horizontally stretched, while the solids circulation vortex in the top section of the bed is elongated over almost the entire bed. As the pressure is increased, the net area covering up-flow of solids is increased and the rate of down flow of solids near the wall is increased. This is due to channel flow of bubbles in the center at very high pressure.

A comparison with experimental results shows that our simulations show good agreement with reality. Results on the bubble characteristics are consistent with results reported in the literature. Further experimental work is highly recommended to investigate the solids motion at high operating pressures. This study provides insight into the bubble and solids motion at elevated pressures, which is not easy to achieve with experiments. From this study we can conclude that the two-fluid model can be used to study the scale-up of gas−solids flow at high operating pressures. This study will promote the understanding of complex fluidization behavior at different operating pressures.

dx.doi.org/10.1021/ie502474k | *Ind. Eng. Chem. Res.* 2014, 53, 17487−17498

AUTHOR INFORMATION

Corresponding Author

*Tel: 31-40-247-3674. Fax: 31-40-247-5833. E-mail: J.T.Padding@tue.nl.

Notes

The authors declare no competing financial interest.

ACKNOWLEDGMENTS

The authors thank the European Research Council for its financial support, under its Advanced Investigator Grant scheme, contract number 247298 (Multiscale Flows).

REFERENCES

(1) van Swaaij, W. P. M. Chemical reactor. In *Fluidization*, 2nd ed.; Davidson, J. F, Clift, R., Harrison, D., Eds; Academic Press: London, 1985; pp 592−629.

(2) Beetstra, R.; Nijenhuis, J.; Ellis, N.; van Ommen, J. R. The influence of the particle size distribution on fluidized bed hydrodynamics using high-throughput experimentation. *AIChE J.* **2009**, *55*, 3013−2023.

(3) Weimer, A. W.; Quarderer, G. J. On dense phase voidage and bubble size in high pressure fluidized beds of fine powders. *AIChE J.* **1985**, *31*, 1019−1028.

(4) Olsson, S. E.; Wiman, J.; Almstedt, A. E. Hydrodynamics of a pressurized fluidized bed with horizontal tubes: Influence of pressure, fluidization velocity and tube-bank geometry. *Chem. Eng. Sci.* **1995**, *50*, 581−592.

(5) Wiman, J.; Almstedt, A. E. Influence of pressure, fluidization velocity and particle size on the hydrodynamics of a freely bubbling fluidized bed. *Chem. Eng. Sci.* **1998**, *53*, 2167−2176.

(6) Orta, A.; Wu, B.; Ghods, M.; Guerrero, A.; Bellehumeur, C.; Kantzas, A. Pressure effect on hydrodynamics of a high pressure X-ray transparent polyethylene fluidized bed. *Int. J. Chem. React. Eng.* **2011**, *9*, A97.

(7) Sidorenko, I.; Rhodes, M. J. Influence of pressure on fluidization properties. *Powder Technol.* **2004**, *141*, 137−154.

(8) Olowson, P. A.; Almstedt, A. E. Influence of pressure on the minimum fluidization velocity. *Chem. Eng. Sci.* **1991**, *46*, 637−640.

(9) White, F. M. *Fluid Mechanics*, 3rd ed., McGraw-Hill: New York, 1994.

(10) Chitester, D. C.; Kornosky, R. M.; Fan, L. S.; Danko, J. P. Characteristics of fluidization at high pressure. *Chem. Eng. Sci.* **1984**, *39*, 253−261.

(11) Bin, A. K. Minimum fluidization velocity at elevated temperatures and pressures. *Can. J. Chem. Eng.* **1986**, *64*, 854−857.

(12) Olowson, P. A.; Almstedt, A. E. Influence of pressure and fluidization velocity on the bubble behavior and gas flow distribution in a fluidized bed. *Chem. Eng. Sci.* **1990**, *45*, 1733−1741.

(13) Olowson, P. A.; Almstedt, A. E. Hydrodynamics of a bubbling fluidized bed: influence of pressure and fluidization velocity in terms of drag force. *Chem. Eng. Sci.* **1992**, *47*, 357−366.

(14) Godlieb, W.; Gorter, S.; Deen, N. G.; Kuipers, J. A. M. Experimental study of large scale fluidized beds at elevated pressure. *Ind. Eng. Chem. Res.* **2012**, *51*, 1962−1969.

(15) Brouwer, G. C.; Wagner, E. C.; van Ommen, J. R.; Mudde, R. F. Effects of pressure and fines content on bubble diameter in a fluidized bed studied using fast X-ray tomography. *Chem. Eng. J.* **2012**, *207*−*208*, 711−717.

(16) Darton, R. C.; La Naueza, R. D.; Davidson, J. F.; Harrison, D. Bubble growth due to coalescence in fluidized beds. *Trans. Inst. Chem. Eng.* **1977**, *55*, 274−280.

(17) Ding, J.; Gidaspow, D. A bubbling fluidization model using kinetic theory of granular flow. *AIChE J.* **1990**, *36*, 523−538.

(18) Kuipers, J. A. M.; van Duin, K. J.; van Beckum, F. P. H.; van Swaaij, W. P. M. A numerical model of gas-fluidized beds. *Chem. Eng. Sci.* **1992**, *47*, 1913−1924.

(19) Gidaspow, D. *Multiphase Flow and Fluidization: Continuum and Kinetic Theory Descriptions*; Academic Press: Boston, 1994.

(20) Nieuwland, J. J. Hydrodynamic modelling of gas−solid two-phase flows. Ph.D. Thesis, Twente University, Enschede, The Netherlands, 1995.

(21) Verma, V.; Deen, N. G.; Padding, J. T.; Kuipers, J. A. M. Two-fluid modeling of three-dimensional cylindrical gas−solid fluidized beds using the kinetic theory of granular flow. *Chem. Eng. Sci.* **2013**, *102*, 227−245.

(22) Verma, V.; Padding, J. T.; Deen, N. G.; Bieberle, M.; Barthel, F.; Wagner, M.; Hampel, U.; Kuipers, J. A. M. Bubble dynamics in a 3-D gas−solid fluidized bed using ultrafast electron beam X-ray tomography and two-fluid model. *AIChE J.* **2014**, *60*, 1632−1644.

(23) Van der Hoef, M. A.; Beetstra, R.; Kuipers, J. A. M. Lattice-Boltzmann simulations of low-Reynolds number flow past mono- and bidisperse arrays of spheres: results for the permeability and drag force. *J. Fluid Mech.* **2005**, *528*, 233−254.

(24) Srivastava, A.; Sundaresan, S. Analysis of a frictional-kinetic model for gas-particle flow. *Powder Technol.* **2003**, *129*, 72−85.

(25) Brown, R.; Brue, E. Resolving dynamical features of fluidized beds from pressure fluctuations. *Powder Technol.* **2001**, *119*, 68−80.

(26) Kage, H.; Agari, M.; Ogura, H.; Matsuno, Y. Frequency analysis of pressure fluctuation in fluidized bed plenum and its confidence limit for detection of various modes of fluidization. *Adv. Powder Technol.* **2000**, *11*, 456−475.

(27) Llop, M. F.; Jand, N. The influence of low pressure operation on fluidization quality flow. *Chem. Eng. J.* **2003**, *95*, 25−31.

(28) Godlieb, W. High pressure fluidization. Ph.D. Thesis, Eindhoven University of Technology, The Netherlands, 2010.

(29) Goldschmidt, M. Hydrodynamic modelling of fluidised bed spray granulation. Ph.D. Thesis, Twente University, Enschede, The Netherlands, 2001.

(30) Cai, P.; Chen, S. P.; Jin, Z. Q.; Wang, Z. W. Effect of operating temperature and pressure on the transition from bubbling to turbulent fluidization. *AIChE Symp.* **1989**, *270*, 37−43.

(31) Godlieb, W.; Deen, N. G.; Kuipers, J. A. M. On the relationship between operating pressure and granular temperature: A discrete particle simulation study. *Powder Technol.* **2008**, *182*, 250−256.

(32) Toomey, R. D.; Johnstone, H. F. Gaseous fluidization of solid particles. *Chem. Eng. Progr.* **1952**, *48*, 200.

(33) Hoffmann, A. C.; Yates, J. G. Experimental observations of fluidized beds at elevated pressure. *Chem. Eng. Commun.* **1986**, *41*, 133−149.